PAPER • OPEN ACCESS

Real-time plasma equilibrium reconstruction and shape control for the MAST Upgrade tokamak

To cite this article: H. Anand *et al* 2024 *Nucl. Fusion* **64** 086051

OPEN ACCESS
IOP Publishing | International Atomic Energy Agency
Nuclear Fusion
Nucl. Fusion **64** (2024) 086051 (15pp)
https://doi.org/10.1088/1741-4326/ad5c80

Real-time plasma equilibrium reconstruction and shape control for the MAST Upgrade tokamak

H. Anand[1,*], W. Wehner[1], D. Eldon[1], A. Welander[1], Z. Xing[1], A. Lvovskiy[1], J. Barr[1], E. Cho[1], B. Sammuli[1], D. Humphreys[1], N. Eidietis[1], A. Leonard[1], M. Kochan[2], C. Vincent[2], G. McArdle[2], G. Cunningham[2], A. Thornton[2], J. Harrison[2], V. Soukhanovskii[3] and J. Lovell[4]

[1] General Atomics, San Diego, CA, United States of America
[2] United Kingdom Atomic Energy Authority, Culham Science Centre, Oxfordshire, United Kingdom of Great Britain and Northern Ireland
[3] Lawrence Livermore National Laboratory, Livermore, CA, United States of America
[4] Oak Ridge National Laboratory, Oak Ridge, TN, United States of America

E-mail: anandh@fusion.gat.com

Received 12 January 2024, revised 14 June 2024
Accepted for publication 27 June 2024
Published 8 July 2024

Abstract

Real-time magnetic control has been developed to deliver precise control of multiple plasma shape parameters for advanced divertor configurations, including double-null, Super-X, X-point target and X-divertor for the first time on the MAST Upgrade (MAST-U) spherical tokamak. Successful real-time magnetic equilibrium control of different plasma shape variables has been accomplished in the 2022–2023 MAST-U experimental campaign for the advanced MAST-U divertor configurations. Application of the MAST-U boundary reconstruction algorithm, LEMUR, is described and compared with off-line equilibrium reconstruction and diagnostic measurements. The process of design and verification of the axisymmetric magnetic control schemes using a suite of control analysis tools (known collectively as TokSys) is also described.

Keywords: magnetic reconstruction, magnetic control, real-time, spherical tokamaks, advanced divertors configurations

(Some figures may appear in colour only in the online journal)

1. Introduction

The MAST Upgrade (MAST-U) spherical tokamak [1] has been designed to explore extended- and expanded-leg divertor geometries, including the Super-X [2] and double-null divertor plasma configurations. These advanced divertor configurations are proposed to allow higher-performance core-plasma operations without excessive erosion and/or damage to the divertor target. Hence, accurate control of the novel boundary and divertor magnetic field configuration, including spatial control of the divertor leg extension is mandatory for MAST-U. In addition, control of the plasma boundary ensuring adequate clearance between the plasma and the plasma-facing wall components, while simultaneously maximising the plasma volume within the available space is a crucial asset in MAST-U plasma operation. Prior to late 2022, the MAST-U plasma configurations (Super-X and double-null divertor) were controlled primarily in feedforward mode,

* Author to whom any correspondence should be addressed.

with the exception of plasma outer gap control employing a simplified single-input and single-output (SISO) formalism, used in a few plasma discharges during the MAST-U 2021 experimental campaign. Deviations from the plasma assumptions used in calculating feedforward parameters resulted in departures from the desired magnetic equilibrium in the absence of feedback control in the previous experimental campaign, particularly in scenarios with auxiliary heating and current drive altering the current profile. Controlling the plasma boundary and divertor geometries in feedforward mode often requires tuning over multiple discharges, which can lead to inefficient use of operational machine time, and difficulty sustaining a desired operating point. As a result, configurations such as X-point target [3] and X-divertor [4, 5] were only achieved transiently during the 2021 experimental campaign. Thus, real-time simultaneous feedback control of the full magnetic equilibrium, including the plasma boundary and divertor geometry, is mandatory for optimizing plasma performance for advanced divertor plasma configurations on MAST-U.

The conventional solution for the time-varying, non-linear, multivariable plasma boundary control problem is a solution to an inverse problem for precomputing a set of feedforward coil currents and voltages [6, 7]. Then, typically a set of independent, SISO PID controllers are designed to stabilize the plasma vertical position and control the radial position and plasma current, with the aim of avoiding mutual interference between them. Ultimately, the control architectures are further supplemented by an additional control loop for the plasma boundary, which relies on the implementation of a real-time estimation of the plasma equilibrium [7–9] for feedforward coil current modifications. The plasma boundary controllers are designed on the basis of linearized model dynamics [10–17], and then sufficient tracking of the shape control targets are obtained with the help of gain scheduling. The development of the MAST-U plasma boundary controller is based on the same concept, where the controller design is determined by the pseudo-inverse of the static gain of the perturbed equilibrium plasma response model [18], with poloidal field coil currents as inputs and outputs as shape control target control variables. A local higher order expansion of poloidal flux calculations constrained by the vacuum field equation, fitted to the magnetic field and flux measurements provides the necessary information for the real-time boundary and divertor geometry estimation on MAST-U tokamak [19–21]. Similar techniques based on local flux expansion methods have already been used successfully for plasma boundary reconstruction on the JET and EAST tokamaks [9, 22]. Although the plasma boundary controllers based on a linearized plasma response are usually effective, they require substantial design, verification and validation, prior to experimental implementation, especially for complex shapes with dynamic evolution. The successful system commissioning of the MAST-U plasma shape controller with minimal on-machine effort was enabled by the Integrated Plasma Control (IPC) approach provided by the General Atomics Tokamak System Toolbox (GA-TokSys) modelling and simulation environment [23]. The generality, flexibility and extensive operational algorithms offered by GA TokSys are routinely used for the development and verification of shape control algorithms for several operating devices, including, DIII-D [24], KSTAR [25], and EAST [26]. It has also been applied to control analysis and design for future tokamaks including ITER [27] and STEP [28].

The main achieved operational parameters of the MAST-U tokamak [29] are the following: major radius 0.7 m, minor radius 0.5 m, vacuum toroidal field up to 0.72 T, plasma current up to 1 MA, elongation up to 2.5, triangularity up to 0.6 and pulse duration up to 1.2 s. Figure 1(*a*) shows the MAST-U poloidal cross-section with an example of a Super-X divertor configuration and poloidal field (PF) coil locations. The P1 coil is used to inductively create the desired toroidal electric field inside the vacuum vessel and drive the plasma current. The solenoidal Pc coil is used for regulating the inner shape of the plasma. Note that the Pc coil is not currently used for shape development and is planned to be commissioned during future MAST-U campaigns. The P4 and P5, up/down symmetric coil pairs are used for providing the plasma boundary shaping field. In addition, 8 up/down symmetric pair coil sets (D1, D2, D3, Dp, D5, D6, D7, Px) are installed in locations around the divertor baffle/plate to support exploration of various divertor configurations, including Super-X and double null plasma configurations. The vertical position control of the most highly elongated ($\kappa \approx 2.4$) MAST-U divertor plasmas is performed with the help of an up/down antisymmetric coil pair, P6. The plasma control system (PCS) for MAST-U inherits most of the original MAST hardware/software architecture, which was based on an architecture developed for DIII-D [29]. The generic software infrastructure from DIII-D has been retained for MAST-U but the tokamak-specific algorithm software has been re-written to support the additional capabilities of MAST-U, including PF coil current control. The details of the functional implementation of the PF coil current controller relevant to this work can be found in [29]. The extensive poloidal-field coil system, flexible PCS, along with the recent successful implementation of LEMUR [21] on MAST-U have paved the way to the design of a new real-time magnetic equilibrium controller for advanced divertor configurations such as double-null and super-X divertors.

The paper is structured as follows. Section 2 describes the MAST-U boundary reconstruction algorithm (LEMUR), verification and validation of the algorithm against off-line equilibrium reconstruction (EFIT), and diagnostic measurements for MAST-U. Section 3 describes the design and verification of the new MAST-U magnetic equilibrium controller with the help of IPC closed-loop scenario simulation using GA-TokSys. Examples of the experimental implementation of the equilibrium controller on MAST-U for double null, super-X, X-point target and X-divertors are discussed in section 4. A summary and outlook for the applications of the controller for enabling future advanced plasma configurations on MAST-U is provided in section 5.

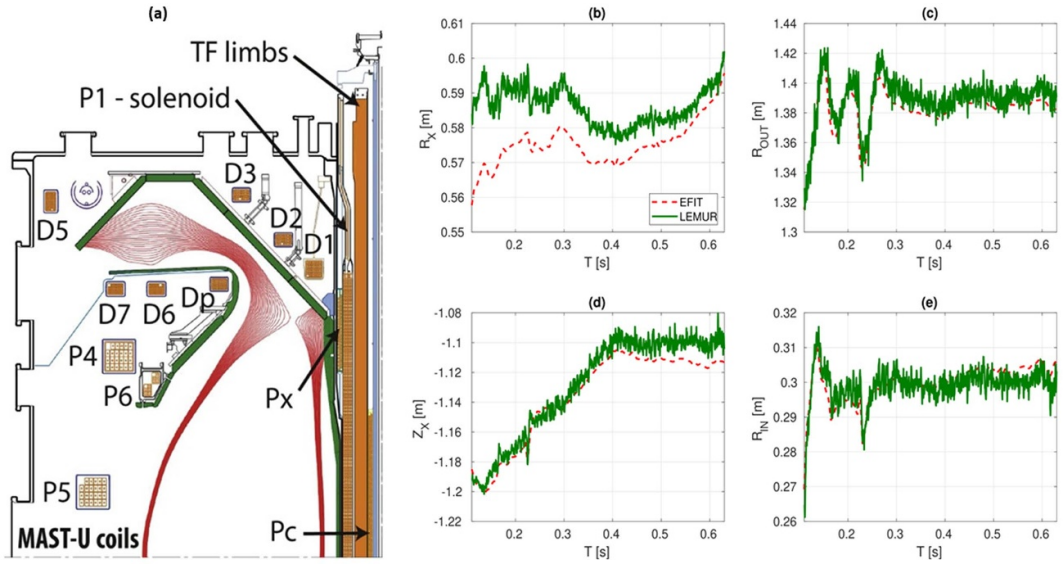

Figure 1. (*a*) MAST-U upper left vessel cross-section showing Super-X divertor flux surfaces and PF coil locations Reproduced from [5]. © 2020 IAEA, Vienna . All rights reserved. (*b*)–(*e*) Comparison between the plasma boundary parameters from real-time LEMUR and off-line EFIT for MAST-U plasma discharge, #46578.

2. Local expansion MAST-U reconstruction algorithm

Plasma magnetic equilibrium control on MAST-U is comprised of the identification of the plasma boundary in real-time and adjustment of the PF coil currents to bring the real-time equilibrium parameters as close as possible to the pre-programmed references. The recent deployment of the real-time LEMUR algorithm [21] has fulfilled a necessary requirement of the real-time estimation of shape and divertor parameters for the development of a real-time magnetic equilibrium control algorithm. LEMUR and other similar real-time equilibrium codes [9] provide an approximate magnetic reconstruction based on the local expansion of poloidal flux constrained by the vacuum field equation, fitted to the local magnetic field and flux measurements in the vicinity. The coefficients of expansion are determined by imposing the vacuum magnetic field equation and by fitting to the local poloidal flux values from the flux loops and magnetic field measurements from the pickup coils on MAST-U. The local expansion method was chosen due to the real-time part of the algorithm being able to fit the required parameters in deterministic time without need to rely on an iterative method, and due to its successful application in the JET tokamak plasma control system [9]. The complete details of the reconstruction method, along with application and assessment of the performance of the technique on a long-legged divertor plasma configuration and benchmarking against experimental diagnostic data on an operating device—the DIII-D tokamak are reported in [20]. Note that, LEMUR had already been implemented as a MAST-U PCS algorithm prior to this work, the re-implementation on DIII-D provided validation and for data provenance with respect to the long-legged divertor configuration before actual experimental application during the MAST-U campaign. Followed by the successful experimental validation on DIII-D, the method was used successfully for real-time plasma boundary reconstruction for different plasma configurations since the 2022–2023 MAST-U experimental campaign [21]. The LEMUR algorithm was implemented on the MAST-U Plasma Control System (PCS) [29] and achieved sub-ms (∼0.5 ms) computational performance (with 1.0 ms extra lag due to analogue input signal smoothing). Prior to the real-time experimental application, the LEMUR method has been extensively validated against the off-line plasma boundary reconstruction algorithm, based on the solution to the Grad–Shafranov equation, EFIT [30, 31], for multiple MAST-U plasma discharges, including double null and Super-X plasma configurations. The verification of the radial, (R_X) and vertical (Z_X) X-point position, radial coordinate of the inner (R_{IN}) and outer gap (R_{OUT}) at the mid-plane from LEMUR is performed by comparing with the associated reconstruction boundary variables derived from the off-line EFIT method for multiple discharges performed during the MAST-U experimental campaign. An example of the LEMUR application to a double null MAST-U plasma with a conventional divertor configuration, #46578, for the determination and comparison of the plasma discharge parameters with respect to off-line EFIT is shown in figures 1(*b*)–(*e*). The difference in the performance of LEMUR with respect to EFIT is found to be comparable for all boundary control variables. Figures 1(*b*) and (*d*) shows a small variation (<2 cm) between EFIT vs. LEMUR, thereby demonstrating a similar performance with respect to the estimation of the X-point position during the plasma evolution. In addition to the good agreement in the X-point positions between LEMUR and EFIT, the LEMUR estimation of the inner/outer plasma gaps

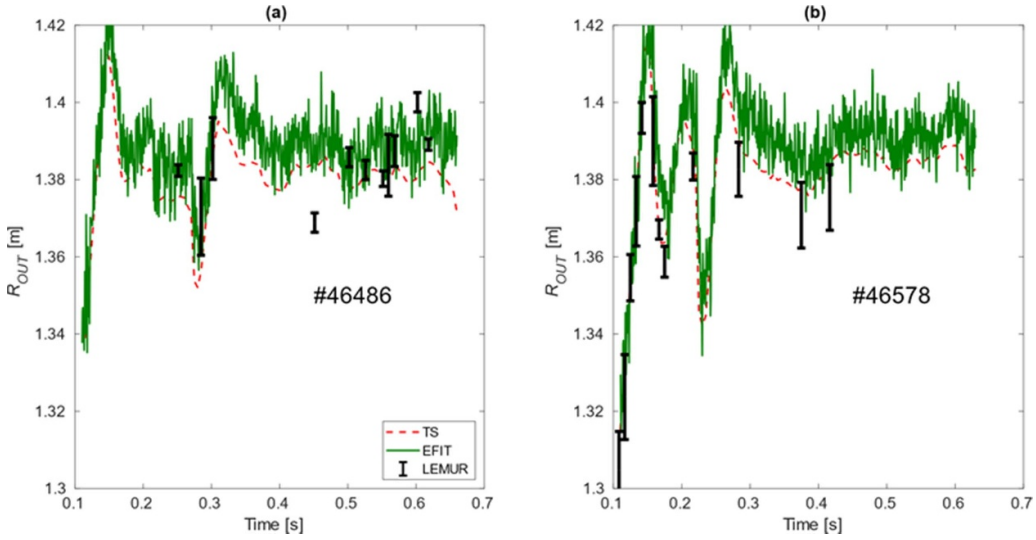

Figure 2. (*a*)–(*b*) Comparison of LEMUR reconstruction (EFIT included for reference) with Thomson scattering data for MAST-U plasma discharge #46486 and #46578. The electron temperature, T_e on the last closed flux surface is expected to lie within 20–40 eV. The error bars show the range of R_{OUT} between radial positions corresponding to pedestal temperatures $T_e = 20$ eV and $T_e = 40$ eV, respectively.

compares well with respect to the EFIT parameters. As shown in figures 1(*c*) and (*e*), a small difference for R_{IN} and R_{OUT} with a maximum deviation <1 cm is observed, indicating that LEMUR can work as well as the off-line EFIT in determining the plasma gaps during the plasma evolution.

In addition to the verification against off-line EFIT, efforts for validating various LEMUR parameters against experimental data derived from different boundary diagnostics of MAST-U that are not input to LEMUR or EFIT have also been performed. For example, efforts to benchmark the LEMUR estimation for the proximity of the plasma boundary with the MAST-U outer wall against the diagnostics data from Thomson Scattering (TS) measurements are shown in figures 2(*a*) and (*b*) for two different MAST-U plasma discharges. The R_{OUT} estimated with LEMUR is verified using the electron temperature, T_e, diagnostics data of mid-plane radial profiles from TS measurements. For a typical MAST-U plasma discharge, T_e, at the last closed flux surface is expected to lie within a range of 20–40 eV. Figures 2(*a*) and (*b*) shows the TS estimated range of R_{OUT} that corresponds to pedestal temperature range in between $T_e = 20$ eV and $T_e = 40$ eV for MAST-U plasma discharges (based on global power balance arguments, similar to [32]), #46486 and #46578, respectively. A good comparison in R_{OUT} from LEMUR and the TS diagnostic data was observed as shown in figures 2(*a*) and (*b*), with the LEMUR reconstruction tracking well the midpoint of the plausible range estimated by TS measurements with 1–2 cm for the evaluated shots. The estimated values depend on the sensors selected as reconstruction input and expect to optimise the sensor selection from time to time, therefore the tracking error with EFIT and LP may improve in the future. The location of the flux loops and the pickup coils used by LEMUR for reconstructing R_{OUT} based on the local poloidal flux values and magnetic measurements are shown in figure 3(*c*). A comparison of the radial location of the outer strike point estimated with LEMUR against EFIT and divertor diagnostics on the MAST-U has also been successfully performed for various MAST-U plasma discharges. The main MAST-U divertor diagnostics used for the experimental benchmarking of LEMUR are the Langmuir Probes (LP) [33], Infrared Camera (IR) and Multi-Wavelength Imaging (MWI) camera [34]. Complete details with respect to benchmarking of LEMUR with EFIT and diagnostic data with respect to boundary and divertor shape control variables on MAST-U are reported in [21]. Associated to the divertor leg control, LEMUR estimated R_{STK} shows fast response dynamics and tracking against the experimental derived outer strike point position from LP, IR and MWI diagnostics for a typical MAST-U Super-X plasma discharge involving a full sweep of the leg in the divertor region [21]. For a device of MAST-U size, LEMUR algorithm satisfies the accuracy requirement for shape and divertor quantities, which is $<$2–3 cm and is typically $\sim$1%–2% of the minor radius of the tokamak. The successful validation of LEMUR with the off-line EFIT and with different diagnostics data justifies the PCS implementation and usage of LEMUR for real-time identification of the plasma shape and divertor parameters for feedback control. Key aspects of system integration, testing and verification of real-time performance are reported in [29]. Note that LEMUR MAST-U implementation presently provides real-time estimation of the plasma boundary (R_X, Z_X, R_{IN} and R_{OUT}) and radial strike point position (R_{STK}) spanning conventional double null and Super-X divertor leg regions. LEMUR is constantly under development and for future campaigns plans to include real-time estimations of divertor flux expansion [35], plasma inductance, l_i and plasma performance as described by poloidal beta, β_p. Full details of the future plans with respect to LEMUR can be found in [21].

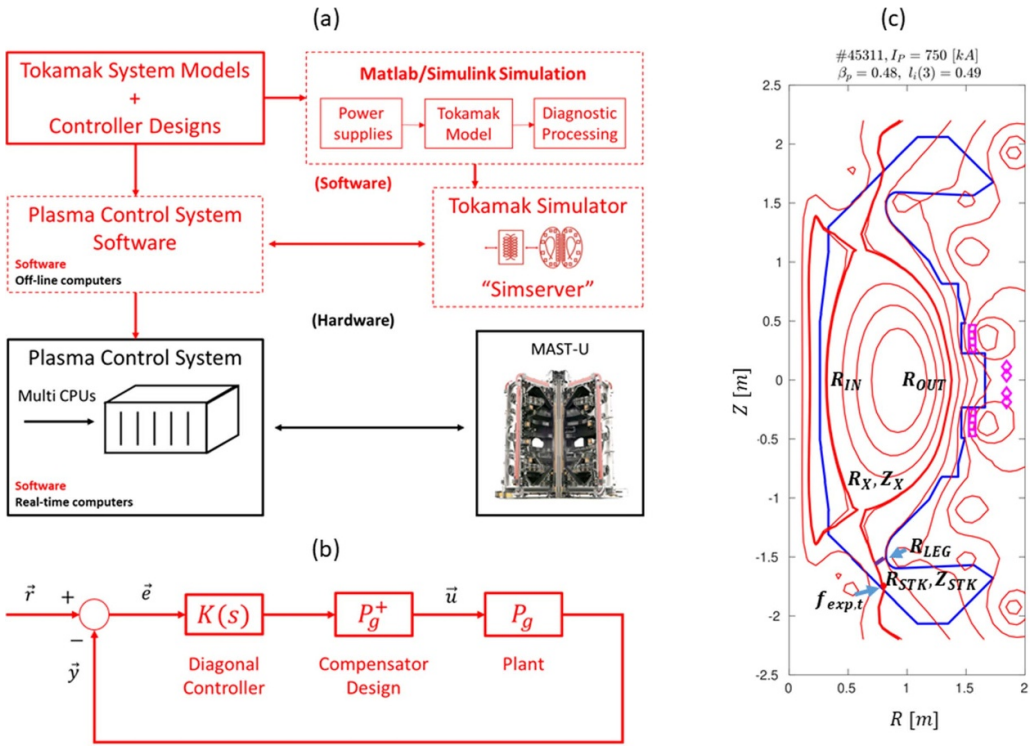

Figure 3. (*a*) MAST-U TokSys environment including the modeling environment is shown in the top boxes. MAST-U model-based closed-loop simulation environment is shown in the middle boxes. The actual MAST-U PCS/Tokamak closed-loop system is schematically shown in the bottom two boxes. (*b*) Simplified block diagram representation of plasma shape control algorithm for MAST-U. (*c*) MAST-U poloidal cross-section showing the conventional double null plasma magnetic equilibrium obtained with off-line EFIT, along with the location of the magnetic shape control variables. The magenta squares and diamonds give the position of the flux loops and magnetic probes used by LEMUR for reconstructingR_{OUT}.

3. Magnetic equilibrium control design and simulation with TokSys

An integrated plasma control approach with the GA-TokSys [23] modelling and simulation environment is used for design and verification of axisymmetric magnetic controllers for the MAST-U tokamak. The TokSys environment, implemented in Matlab and Simulink, provides physics-based models validated by experimental results for construction of axisymmetric control models and facilitates design of relevant controllers. The environment provides direct connection to the MAST-U PCS [29] through the generation of model-based simulation servers (simservers) and allows detailed simulation of the PCS/power supply/plasma system [23]. The architecture of the MAST-U simulation environment in a schematic form is shown in figure 3(*a*). Model development and scenario, and controller design are accomplished in the upper blocks in figure 3(*a*). Once controller and scenario design are prescribed and the controller is implemented within the MAST-U PCS, a complete software-in-the-loop (SIL) closed-loop simulation of the PCS/model-based simserver can run with functionality identical to that of the actual MAST-U PCS controlling the tokamak (middle boxes in figure 3(*a*)). The simserver can contain a simple vacuum model or a linearized or non-linearized plasma model based on EFIT plasma reconstruction [36, 37]. MAST-U PCS interface, data acquisition storage, and visualization methods are identical to that of an actual plasma discharge. This environment allows debugging of the entire system, including controller verification prior to operation on the MAST-U tokamak. This functionality is indispensable for enabling MAST-U magnetic equilibrium control development and has resulted in minimal on-machine tuning effort for plasma operations on MAST-U.

Figure 3(*b*) shows the simplified block diagram for the architecture of the plant used for the design of the MAST-U plasma magnetic equilibrium controller. It is a multiple input and multiple output (MIMO) system with PF coil currents as inputs and the shape controlled variables as outputs. A non-diagonal plant matrix, P_g is defined, where a change in its input would affect all its outputs. Consequently, a compensator P_g^+, the pseudo-inverse of the static gain of the plant, is derived, provided that P_g has full rank in the output space, to counteract the interaction of the plant. The result is a 'newly' shaped plant, $P_gP_g^+$, which is nearly diagonal and easier to control than the original plant P_g. A diagonal proportional and integral controller $K(s)$ is utilised, with diagonal gain matrices to be designed. The above method of the shape control design is common to many tokamaks (DIII-D, NSTX-U, TCV, JET, KSTAR and EAST) and has been replicated on each of these devices routinely for equilibrium control. The current implementation on MAST-U differs only at the level of the shape control variables. The mentioned devices with advanced real-time equilibrium codes host shape control design based on real-time estimations of plasma gaps, poloidal

flux at the target boundary points, multiple X-points and strike points, along with direct shape parameters (elongation, triangularity and squareness). However, as mentioned earlier the real-time LEMUR code is currently limited to estimating a specific subset of variables (R_X, Z_X, R_{IN}, R_{OUT} and R_{STK}) and thus restricts the shape control design to these quantities for now. The MAST-U shape controller has been designed to perform the following task: track step and ramp references on the controlled variables: 2–10 cm on the shape control variables with settling times between $\approx$ 10–30 ms, respectively. In addition, the controller design should be based on the shape control variables that are currently estimated in real-time by the LEMUR reconstruction code (R_{OUT}, R_{IN}, R_X, Z_X and R_{STK}) with the flexibility to extend to a larger set of control variables. A frequency separation approach is adopted to solve the plasma magnetic control problem for MAST-U. With this approach, the plasma is vertically stabilized on the fastest time scale ($\leq$1 ms) accessible with the passive structures, P6 coils, and fast power supplies. The shape controller operates on a slow loop and is designed on the basis of the stable system obtained by taking into account the vertical stabilization controller. The plant matrix, P_g, for controller design is generally obtained with the help of the linear plasma response model based on the solution to a perturbed Grad–Shafranov equation [36] and defines the static relationship between PF coil currents and equilibrium control variables estimated from LEMUR as shown in figure 3(c). In addition to the shape variables shown in figure 3(c), the plant matrix has the flexibility for expansion to account for additional control variables, such as the radial coordinate corresponding to the intersection of the separatrix and a segment across the divertor nose, R_{LEG}, divertor flux expansion, $f_{\mathrm{exp},t}$ defined as the ratio of the distance between the same flux surfaces at the divertor target and at the outer-midplane, as well as new shape variables expected to be estimated by LEMUR in future. In addition to the definition of the primary X-points, the plant matrix can also host additional X-points to extend equilibrium control development architecture to X-divertor and X-point target divertor plasma configurations [3–5]. Similar to the control of the plasma vertical position, the MAST-U shape controller design relies on a separate independent loop for the control of the plasma current with the P1 PF coil and does not include terms for minimizing the perturbation to the plasma current during control of the shape variables. In addition to the above limitation, the controller design also does not include constraints for respecting the hardware limits of the PF coils. This may result in large coil current demands exceeding the PF coil current limits or may appear in the form of dipoles, i.e. positive and negative currents in adjacent coils. In addition, the MAST-U shape control design also does not account for respecting the force limits and total resistive power dissipation in the PF coils. As mentioned before, the Pc PF coil for R_{IN} control is currently not available on MAST-U. The shape controller takes that into account and generates actuator directions for controlling R_{IN} and R_X, both of which heavily depend on the use of the Px coil. This can ultimately result in a situation where to provide greater allowance for the feedback control of R_{IN}, R_X will have to be kept in open loop in order to reduce demand and prevent exceeding the current limit on the Px coil. As the compensator matrix, P_g^+ is only valid on the plasma magnetic equilibrium around which the linearization is performed, the performance of the shape controller design is expected to degrade for plasma magnetic equilibria that are very different from the point of linearization. This limits the application of the shape controller and requires generation of a new P_g^+ based on the plasma configuration to be controlled. Another consequence of the present shape controller design is its impact on the shape variables that are not included in the definition of the plant matrix. This may result in undesirable perturbations of these variables that are absent in the plant definition during the control of the chosen set of the shape variables. However, including a larger set of variables in the plant definition may also result in large PF coil current demands. Thus, as expected a trade-off in the present design is made based on controlling a limited set of control variables which provides an overall control of the plasma shape while avoiding large PF coil currents exceeding the hardware limits.

In particular, if $\delta\vec{y}$ represents the variations in the boundary and divertor control variables estimated with LEMUR and $\delta\vec{u}$ are the PF coil currents then: $\delta\vec{y} = P_g\delta\vec{u}$. Consequently, the magnetic equilibrium controller design then follows:

$$\delta\vec{I}_{PF} = P_g^+ K(s)\ \vec{e} \tag{1}$$

where, $\delta\vec{I}_{PF}$ are the PF current request to the MAST-U PF coil current controller, $\vec{e}$ represents the associated errors in the magnetic control variables and s is the Laplace transform variable. Note that, P1 and P6 poloidal field coils are excluded in the design since they are used for plasma current and vertical position control and stabilization, respectively. In addition, the Pc coil is also not included in the design due to its unavailability in the present MAST-U campaign. In terms of MAST-U PCS terminology [29], the column vectors of P_g^+ represent 'virtual circuits' that are assembled into a transformation matrix which maps the vector of the virtual actuator requests to a vector of PF coil currents in the PCS. The complete details of the functional flow of the MAST-U magnetic equilibrium controller requests to the MAST-U PF coil current controller can be found in [29]. The MAST-U PCS also offers the flexibility to program the use of the 'virtual circuits' in different control modes, feedforward or feedback. In case of the feedforward mode, 'virtual circuits' defined as the PF coil currents required in each coil to change a given magnetic control variable by one unit, are directly driven by the perturbation in the control variable itself defined by the PCS programmer. However, in case of the feedback mode, the perturbation represents the error in the magnetic control variables and is directly supplied in real-time from the LEMUR algorithm.

The verification of the MAST-U equilibrium controller is performed with the help of a non-linear free-boundary simulation code, GSevolve [36]. This simulation code evolving the Grad–Shafranov equilibrium including current and pressure profiles resides within the suite of TokSys tools.

The unique capability of the software suite to directly connect to the MAST-U PCS via SIL provides simulated tokamak and plasma data in response to the control commands

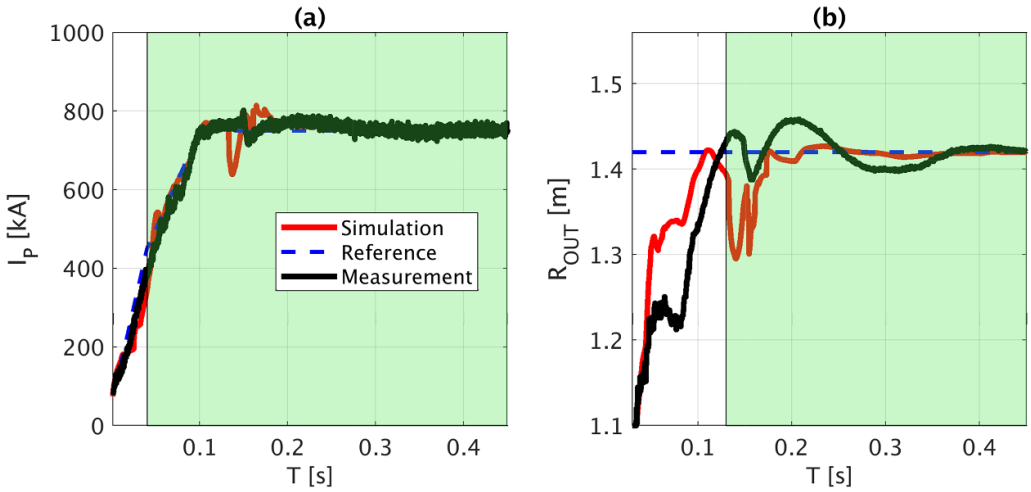

Figure 4. Performance of the magnetic controller with respect to R_{OUT} control during GSevolve simulation. Comparison between the simulation, measurement and the reference for (*a*) plasma current, I_P and (*b*) R_{OUT} for plasma discharge, #45311. The activation time intervals of the plasma current controller and the outer gap controller are shown by the shaded regions in green.

from the shape controller (figure 3(*a*)). The closed-loop simserver simulations help to tune controller gains and confirm the implementation and operation under realistic hardware/software conditions. GSevolve simulations have been performed based on a conventional double null MAST-U plasma magnetic equilibrium, #45311, as shown in figure 3(*c*). In addition to the verification of the general implementation of the magnetic controller on the MAST-U PCS, the simulations are also aimed at identifying the first initial guess for the control parameters that results in good response (≈30–50 ms) and tracking with low steady state error (≈1–2 cm). For the verification of the implementation of the MAST-U magnetic controller for the given plasma equilibrium, a controller corresponding to R_{OUT} is activated at a specific time interval during the full discharge simulation. The PF coil controller and plasma current controller are fed with the same MAST-U PCS configuration parameters as in the original shot #45311 throughout the GSevolve simulation, while the plasma magnetic equilibrium controller for R_{OUT} is now activated at a given time instant, $T = 0.13$ s, during the simulation. The performance of the plasma shape is evaluated by studying the response of the R_{OUT} for an arbitrary step reference waveform. Figures 4(*a*) and (*b*) shows the application of the magnetic controller for controlling the plasma outer gap from $T = 0.13$ s, during the GSevolve simserver simulation with the MAST-U PCS for the plasma discharge, #45311, shown in figure 3(c). The activation interval along with the other settings associated with the plasma current controller are set automatically by restoring MAST-U PCS configuration used in the original shot #45311. The shaded region in green in figure 4(*b*) shows the step response performance of R_{OUT} upon activation at $T = 0.13$ s. Smooth tracking of the pre-programmed reference with a response time of ≈30–50 ms and a small steady state error (≈1 cm) is achieved for R_{OUT}. Figure 4(*a*) shows the response of I_P during the GSevolve scenario simulation with the designed magnetic controller regulating the plasma outer gap. Figure 4(*a*) shows plasma current controller tracking and the disturbance rejection performance with respect to the transients induced by the activation of plasma magnetic controller loop. Figures 4(*a*) and (*b*) also show the comparison of the GSevolve simulations against the measured I_P and R_{OUT} for the plasma discharge, #45311. The dynamic responses during the simulation of both the variables show differences in comparison to the real shot. The differences in the responses are consistent with those commonly observed when simplified models (first order system with an associated time constant, delay and saturation limits) for the power supplies are used as in this case. Another potential source of these discrepancies is the omission of the experimentally consistent noise in the simulation used in reconstructing the control variables. The present simulation simply used ideal magnetics data directly obtained from the plasma model itself without addition of a noise component. The models of the power supplies and magnetic diagnostics are already planned for validation against experimental data during the upcoming MAST-U experimental campaign, in order to better identify the actual sources of discrepancies. However, even with these limitations the closed-loop simserver simulation framework plays an essential role for debugging, testing, verifying and assessing off-line the response of the virtual circuits prior to shot execution. The simulations provide significant confidence in achieving satisfactory response during the first experimental implementation.

4. Experimental application of the plasma shape controller

Similar to the verification process discussed in the previous section for the plasma magnetic equilibrium controller for R_{OUT}, additional tests are carried out for evaluating the performance of the other boundary and divertor control variables with the 'simulation server' using the non-linear free-boundary simulation code, GSevolve. After validating the performance in simserver simulation, dedicated experiments have

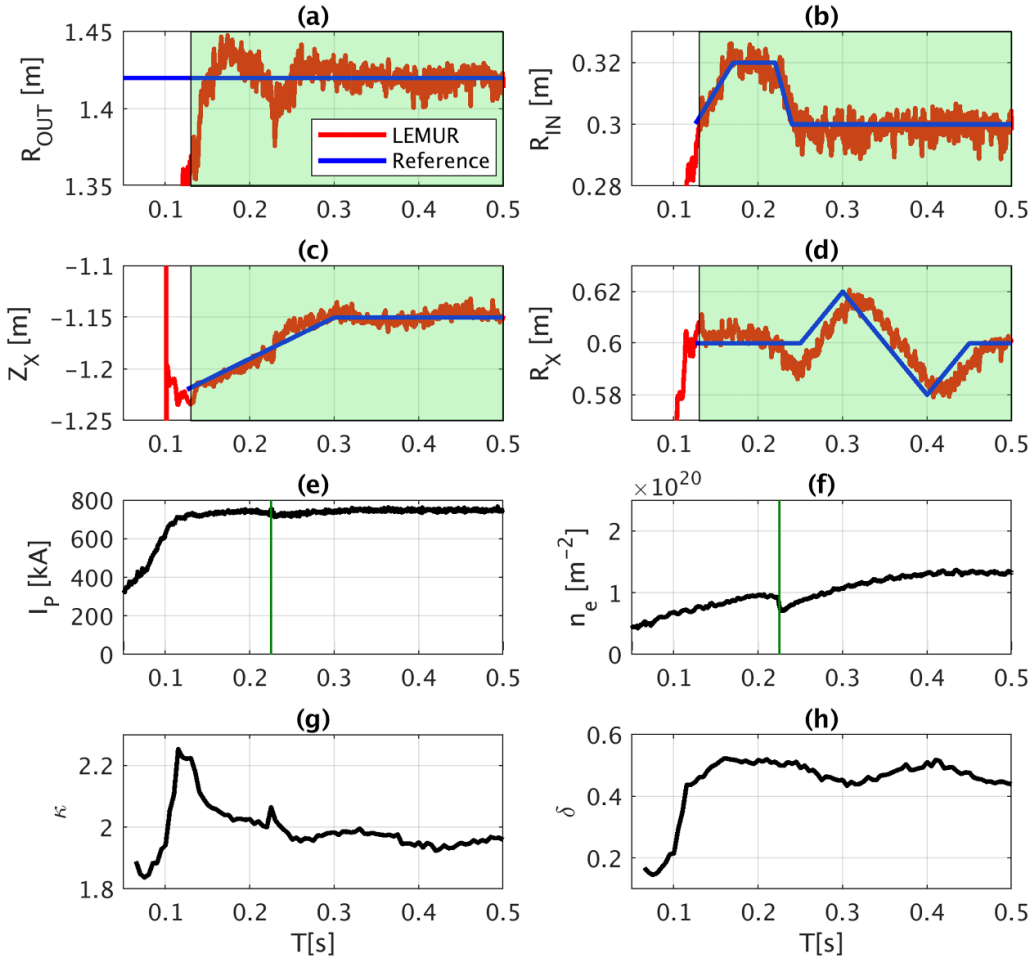

Figure 5. Performance of the shape controller for a MAST-U double null plasma configuration, #46226, involving a scan of the plasma inner gap and X-point position. Comparison between the measurement estimated with LEMUR (red) and the reference (blue) for (*a*) R_{OUT}, (*b*) R_{IN}, (*c*) Z_X and (*d*) R_X. Time evolution of (*e*) I_P, (*f*) line integrated plasma density, n_e, (*g*) plasma elongation, κ and (*h*) plasma triangularity, δ. The activation time interval of the shape controller is shown by the shaded region in green. The solid green lines in (*e*) and (*f*) correspond to the IRE event time.

been performed to test the plasma magnetic controller during the MAST-U campaign in 2022–2023. The analysis of the experimental results is divided into four main sub-sections, with each sub-section describing the experimental application of the new equilibrium controller design on a MAST-U double null, Super-X, X-point target and X-divertor plasma scenario, respectively.

4.1. Application to double null conventional divertor plasma configuration

MAST-U double null divertor plasma discharges with different plasma currents (450 kA and 750 kA), involving dynamic changes in the reference trajectories of various boundary control variables are chosen to test the magnetic equilibrium controller performance. The equilibrium controller design is formulated by including response vectors based on the plasma equilibrium (figure 3(*c*)), mapping the inner/outer plasma gaps and the X-point position from the PF coil currents. The 'virtual circuits' for the shape variables, R_{OUT}, R_{IN}, Z_X and R_X are then determined by taking the pseudo-inverse of the plant matrix, P_g, comprised of the various shape response vectors. The equilibrium controller design for the double null divertor configuration is implemented in feedback mode in the MAST-U PCS with the help of the 'virtual circuits'. During the real-time application, the error associated with the shape control variables estimated by LEMUR drives the respective 'virtual circuits' for feedback control of the double null divertor plasma configuration.

Figures 5(*a*)–(*d*) show an example of the experimental application of the equilibrium controller for the first time on MAST-U providing real-time feedback control of the radial position of the inner/outer plasma gap and radial and vertical position of the X-point for a 750 kA double null divertor plasma configuration, #46226. The shape of the double null divertor plasma configuration used for testing the controller is similar to the plasma equilibrium shown in figure 3(c). Prior to the present implementation, double null divertor plasma configurations were primarily controlled in feedforward mode on MAST-U. Note that the LEMUR algorithm in the MAST-U PCS is enabled at $T = 0.11$ s. The plasma equilibrium

controller activation time interval for studying the dynamical response with respect to the boundary control variables is represented by the green shaded regions in figures 5(*a*)–(*d*). Overall good tracking performance with respect to the pre-programmed references for all the associated boundary control variables is achieved with a response time of ≈20–30 ms and a small steady state error (≈ 2 cm). Figures 5(*a*) and (b) shows the closed loop performance for regulating the radial position of the outer and inner plasma gap. As shown in figure 5(*a*), the controller exhibits good disturbance rejection and forces the R_{OUT} controlled variable to track the desired reference after a perturbation at $T = 0.255$ s most likely due to an Internal Reconnection Event (IRE) [38]. These are a known artefact of the spherical tokamak aspect ratio (due to the high safety factor gradient relative to conventional aspect ratio tokamaks) and can be characterised by a relaxation of the current density profile resulting in a current spike and crash in the density. The data quality and diagnostic set available at the beginning of the second MAST-U campaign make it difficult to show the current density profile, but the plasma current and the line integrated density identifiers are shown in figures 5(*e*) and (*f*). Figures 5(*e*) and (*f*) shows the IRE characteristics in pulse 46226 with a small spike in plasma current and a crash in density at 0.225 s, correlating with the disturbance in the controlled shape parameters. Figure 5(*b*) demonstrates the application of the controller for preventing contact of the plasma boundary with the inner wall limiter and maintains a suitable distance between them at steady state. The closed loop tracking performance corresponding to the vertical and radial control of the X-point position is shown in figures 5(*c*) and (*d*). A delayed response with a characteristic time delay ≈10–15 ms is observed in the ramp response of radial position of the X-point (figure 5(*d*)). The LEMUR estimated X-point position controlled variables follow the time varying reference trajectory with the activation of the controller and are then kept close to the reference trajectories, providing satisfactory tracking of the radial and vertical position of the X-point (figures 5(*c*) and (*d*)). The experimental impacts of the real-time feedback control of R_{OUT}, R_{IN}, Z_X and R_X on actual plasma shape quantities (plasma elongation, κ, and triangularity, δ), are shown in figures 5(*g*) and (*h*). Figures 5(*g*) and (*h*) also show the response on the plasma elongation and triangularity during the ramp in R_X from 0.3 s–0.4 s when R_{OUT}, R_{IN} and Z_X are held constant. During this interval, the relative elongation change is very small ∼1%. The associated change in triangularity increase is of the order of 10% and relates to the inward radial movement of the X-point. This is expected since R_X is coupled to plasma triangularity when R_{OUT}, R_{IN} and Z_X are held constant.

4.2. Application to Super-X divertor plasma configuration

After successfully testing the MAST-U equilibrium controller design on double null divertor plasma configuration, the controller design was extended experimentally to the super-X plasma configuration with different plasma currents (450 kA and 750 kA). Similar to the double null conventional divertor configuration, the magnetic equilibrium controller performance was evaluated by dynamically changing the reference trajectories for boundary and divertor leg control variables. In contrast to the equilibrium controller design for the double null divertor case, the response matrix is generated for the Super-X plasma equilibrium as shown in figure 6(*g*) and includes the addition of the divertor nose control variable, R_{LEG}, that regulates the proximity of the separatrix with divertor baffle. The design for the equilibrium controller also includes substitution of R_X with R_{STK} in the controller response matrix to regulate the outer strike point position of the long-legged divertor Super-X plasma configuration. During the controller application, an intentional disturbance by varying the divertor flux expansion is included to assess the robustness of the controller with respect to disturbance rejection. Similar to R_{LEG}, the PF 'virtual circuit' for $f_{\mathrm{exp},t}$ is determined by including the response vector, mapping the flux expansion variable at the divertor leg with the PF coils in the controller design. The disturbance in $f_{\mathrm{exp},t}$ is then programmed in the MAST-U PCS in feedforward mode by driving the $f_{\mathrm{exp},t}$ 'virtual circuit' with a user-defined perturbation during the time interval corresponding to the activation of the outer strike point control.

Figures 6(*a*)–(*g*) show an example of the experimental application of the magnetic equilibrium controller for the first time providing real-time feedback control of the plasma boundary (R_{OUT}, R_{IN}, Z_X) and divertor leg (R_{STK}) for a 750 kA Super-X divertor plasma configuration, #47577, on MAST-U. The associated boundary and divertor control variables for the Super-X control are supplied as inputs to the controller from the LEMUR algorithm starting, $T = 0.11$ s, expect for R_{STK} starting at $T = 0.41$ s. The difference in the activation times is due to the fact that for now R_{STK} reconstruction from LEMUR does not cover the entire divertor contour as a function of time and the estimation is only active when the divertor leg scans the divertor tile region corresponding to a conventional double null or Super-X divertor configuration. The activation time interval for studying the dynamical response of the equilibrium control variables with respect to time varying reference waveform is shown in the green shaded regions in figures 6(*a*)–(*d*). The activation for the control variables (R_{IN} and Z_X) starts at $T = 0.13$ s, while the activation of the controller associated with R_{STK} was pre-programmed from $T = 0.45$ s. The activation interval of the feedback controller for R_{OUT} starts at 0.2 s. Figures 6(*e*) and (*f*) explores the effect on the $f_{\mathrm{exp},t}$ and R_{LEG} during the controller operation for regulating the super-X equilibrium. Figures 6(*a*)–(*d*) illustrates good tracking of the time varying pre-programmed reference of all equilibrium control variables upon activation of the controller. Also, the intentional introduction of the pre-programmed $f_{\mathrm{exp},t}$ ramp-down phase (figure 6(*e*)) has negligible effect on the equilibrium controller performance. Smooth tracking performance associated with a low steady state error (≈1 cm) is observed for the boundary control variables, namely, R_{OUT}, R_{IN} and Z_X. Upon activation at $T = 0.45$ s, R_{STK} tracks smoothly the pre-programmed reference, comprising of a ramp-up phase, followed by a constant trajectory and ultimately leads to a small steady state error. Figure 6(*g*) shows the final steady state Super-X magnetic equilibrium achieved after controller

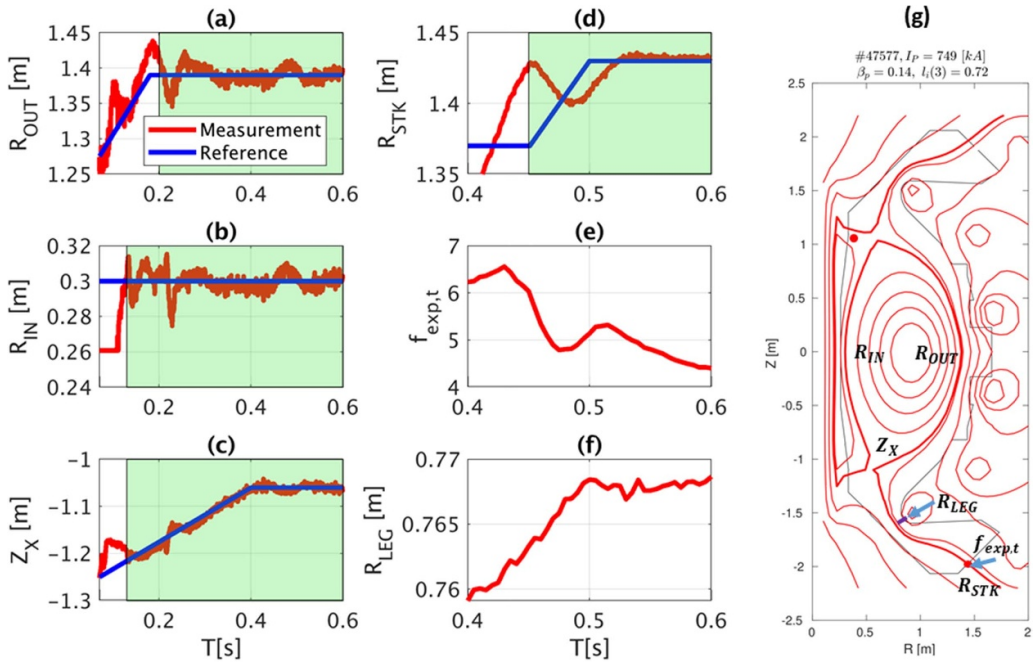

Figure 6. Performance of the shape controller for a MAST-U Super-X plasma configuration, #47577, involving a scan of the vertical position of the X-point and radial position of the outer strike point. Comparison between the measurement (red) estimated with LEMUR and the reference (blue) for (*a*) R_{OUT}, (*b*) R_{IN}, (*c*) Z_X and (*d*) R_{STK}. (*e*) Time evolution of divertor flux expansion at the target, $f_{\mathrm{exp},t}$. (*f*) Time evolution of the radial coordinate of the intersection between the separatrix and the segment across the divertor nose, R_{LEG}. (*g*) MAST-U poloidal cross-section showing the Super-X plasma magnetic equilibrium at steady state after controller operation ($T = 0.6$ s) obtained with off-line EFIT, along with the location of the various magnetic shape control variables. The activation time interval of the shape controller is shown by the shaded region in green. Also, note that the *x*-axis scale of (*d*)–(*f*) differs from (*a*)–(*c*).

termination. In addition to the actively controlled variables, as demonstrated in the figure 6(*f*), the application of the plasma equilibrium controller has minimal impact on $R_{\mathrm{LEG}} \approx$ 1 cm and successfully prevents contact of the plasma separatrix with the divertor baffle and maintains a suitable distance between them at during transients and as well as in steady state.

4.3. Application to X-point target divertor plasma configuration

The X-point target divertor is characterized by a significantly larger X-point separation between the primary and secondary X-points such that the distance between the plasma and the targets is large enough to separate the radiation region from the confined plasma limiting detrimental effects on the plasma performance. Due to unavailability of the secondary X-point position estimation from LEMUR, the equilibrium controller was used in the feedforward mode for introducing a secondary X-point at a user-defined location. The PF 'virtual circuit' for controlling poloidal magnetic field was determined by including the associated response vectors, mapping the radial, B_r and vertical B_z magnetic field components at the specified location, with the PF coils in the controller design. The plant matrix for the X-point target divertor was obtained with the help of a linear plasma response model based on a 750 kA Super-X divertor plasma scenario, #46296, with a shape similar to the one shown in figure 6(*g*). In addition to the boundary control variables (R_{OUT}, R_{IN} and Z_X), the response vectors for generating a poloidal field null at (R, Z) = (1.26 m, −1.83 m) are also included in the plant model based on the perturbed Grad–Shafranov equation. Ramp perturbation waveforms for controlling B_r and B_z to zero at (1.26 m, −1.83 m) are then applied through the MAST-U PCS in the feedforward mode for driving the corresponding 'virtual circuit' regulate the poloidal magnetic field null. The initial value of the ramp waveform in the PCS is set to zero and the final value corresponds to the EFIT pre-computed value of B_r and B_z at the specified location based on the previous discharge. The feedforward control of B_r and B_z components for obtaining the X-point target configuration involves an iterative process and requires tuning of the perturbation waveform over a series of plasma discharges. This is due to the inability of feedforward control to respond to external disturbances during the plasma discharge. The process evaluates the poloidal field components at the specified location using the off-line EFIT plasma equilibrium. These components are then applied as perturbation and the associated virtual circuit acting on these perturbation requests PF coil current changes to compensate and reduce the B_r and B_z values to zero in the subsequent discharge. After the discharge execution, the off-line EFIT code is used again to evaluate the resulting B_r and B_z values at the specified location to update the ramp perturbation based on the remaining poloidal field offset value. The same virtual circuit as the previous discharge is then used

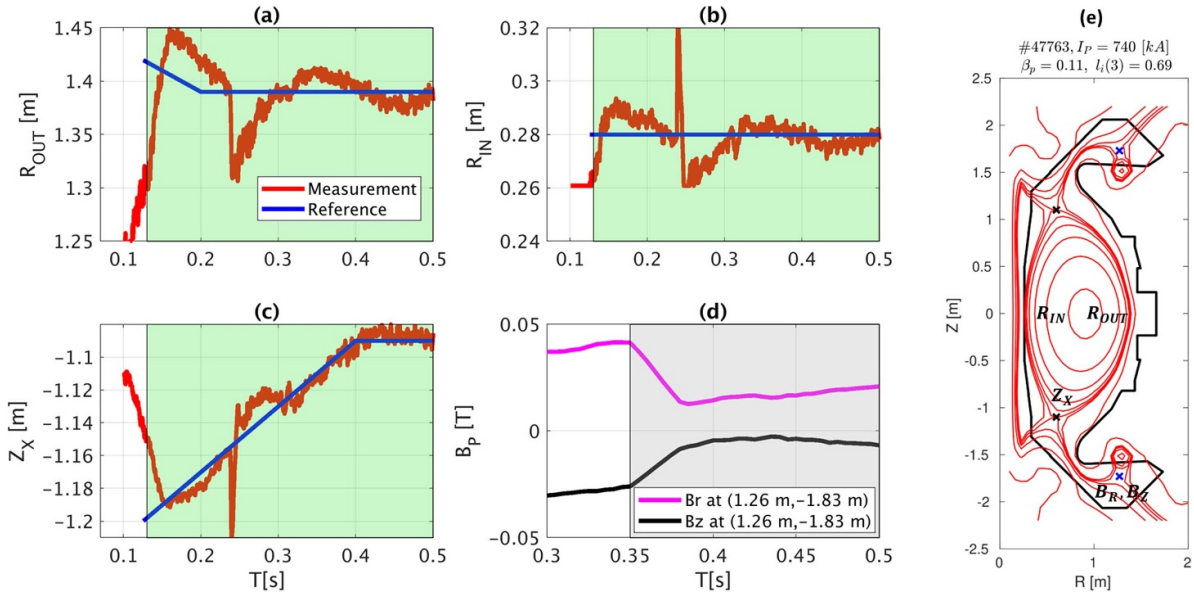

Figure 7. Performance of the shape controller for a MAST-U X-point target plasma configuration, #47763, involving feedback control of R_{OUT}, R_{IN} and Z_X, and feedforward control of poloidal magnetic field at (1.26 m, −1.83 m). Comparison between the measurement (red) estimated with LEMUR and the reference (blue) for (*a*) R_{OUT}, (*b*) R_{IN} and (*c*) Z_X. (*d*) Time evolution of the poloidal magnetic field components at (1.26 m, −1.83 m) from off-line EFIT. (*e*) MAST-U poloidal cross-section showing the X-point target plasma magnetic equilibrium at steady state ($T = 0.5$ s) obtained with off-line EFIT. The activation time interval of the feedback controllers is shown by the shaded region in green and feedforward controllers is shown by the shaded region in grey. Also, note that the *x*-axis scale of (*d*) differs from (*a*)–(*c*).

for requesting the PF coil current changes based on the updated ramp perturbation to converge towards an improved poloidal null in the next discharge.

Figures 7(*a*)–(*e*) show an example of the experimental application of the magnetic equilibrium controller for providing real-time feedback control of the plasma boundary (R_{OUT}, R_{IN}, Z_X) and feedforward control of the poloidal field components at (1.26 m, −1.83 m) for obtaining a 750 kA X-point target divertor plasma configuration, #47763. Note that the resulting performance in the discharge, #47763, was achieved through a sequence of tuning iterations over 3 plasma shots. It must be also noted that this is first time that steady state X-point target divertor plasma configuration has been achieved on MAST-U. The associated boundary control variables are supplied to the feedback controller as inputs from the LEMUR algorithm starting at $T = 0.11$ s. The activation time interval for studying the dynamical response of the boundary control variables (R_{OUT}, R_{IN} and Z_X) is shown in the green shaded regions in figures 7(*a*)–(*c*). Figure 7(*d*) shows the time evolution of B_r and B_z at (1.26 m, −1.83 m) from off-line EFIT reconstruction during the feedforward control operation for regulating poloidal magnetic field components. Figures 7(*a*)–(*c*) shows good tracking of the time-varying pre-programmed reference of all boundary control variables with the activation of the controller. The unintentional introduction of the IRE at $T = 0.23$ s has some transient effect on the equilibrium controller performance, which is ultimately improved over time by the feedback controller. Smooth tracking performance associated with a low steady state error is observed for the boundary control variables. Upon activation of the feedforward controller at $T = 0.35$ s, both, B_r and B_z are ramped towards zero and are held nearly constant thereafter in steady state (figure 7(*d*)). The performance of the feedforward controller reflects the pre-programmed reference values of B_r and B_z perturbation during a phase between $T = 0.35$ s and $T = 0.38$ s, where poloidal magnetic components are ramped from zero and thereafter held constant to the pre-programmed values of B_r and B_z. As mentioned before, the steady state values of the pre-programmed references are determined by evaluating the existing components of B_r and B_z at the desired secondary X-point location from the off-line EFIT of the previous scenario and involve subsequent reference tuning over multiple discharges to achieve a satisfactory level of performance in feedforward control mode. As shown in figure 7(*d*), the poloidal field components with the activation of the feedforward controller reaches very close to B_r and B_z of zero around $T = 0.38$ s but still contains a finite steady state offset, which ultimately show an increasing deviation over time from zero. This is expected during feedforward mode of operation and can be attributed to the inaccurate modelling of the plant and disturbances, and also due to the inability of the controller to respond to random and unforeseen disturbances (e.g. flux swing due to the P1 PF coil). In the future, with the availability of the real-time estimation of the secondary X-point from LEMUR, these 'virtual circuits' can be used in feedback control mode and overcome modelling inaccuracies and achieve good disturbance rejection. Figure 7(*e*) shows the final steady state X-point target magnetic equilibrium achieved after feedback and feedforward controller termination at $T = 0.5$ s. The off-line EFIT reconstruction at steady state estimates the secondary X-point position at (1.27 m, −1.73 m) in comparison to desired location of (1.26 m, −1.83 m).

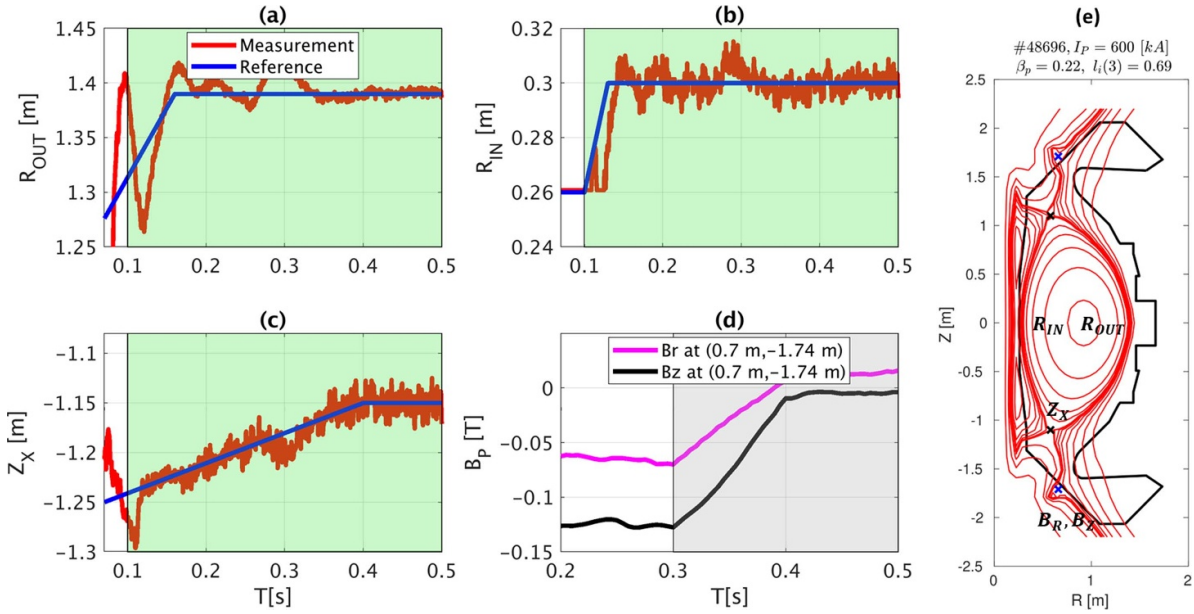

Figure 8. Performance of the shape controller for a MAST-U X-divertor target plasma configuration, #48696, involving feedback control of $R_{\rm OUT}$, $R_{\rm IN}$ and Z_X, and feedforward control of poloidal magnetic field at (0.7 m, −1.74 m). Comparison between the measurement (red) estimated with LEMUR and the reference (blue) for (*a*) $R_{\rm OUT}$, (*b*) $R_{\rm IN}$ and (*c*) Z_X. (*d*) Time evolution of the poloidal magnetic field components at (0.7 m, −1.74 m) from off-line EFIT. (*e*) MAST-U poloidal cross-section showing the X-divertor target plasma magnetic equilibrium at steady state ($T = 0.5$ s) obtained with off-line EFIT. The activation time interval of the feedback controllers is shown by the shaded region in green and feedforward controllers is shown by the shaded region in grey. Also, note that the *x*-axis scale of (*d*) differs from (*a*)–(*c*).

4.4. Application to X-divertor target divertor plasma configuration

The X-divertor concept is characterized by a flaring of the flux surfaces towards the divertor target. The configuration is created by inducing a second axisymmetric X-point downstream of the main plasma X-point near the divertor target. The controller design for X-divertor scenario is similar to the X-point target plasma configuration, with the main difference being with respect to the specification of the spatial location of the secondary X-point. The plant matrix for the X-divertor configuration is obtained by constructing a linear plasma response model based on a 600 kA double-null divertor plasma scenario, #47859, with a shape similar to the one shown in figure 3(*c*). Similar to the X-point target configuration design, the plant model includes the response vectors for the boundary control variables ($R_{\rm OUT}$, $R_{\rm IN}$ and Z_X), along with the vectors for generating a poloidal field null at (R, Z) = (0.7 m, −1.74 m). The 'virtual circuits' for the shape ($R_{\rm OUT}$, $R_{\rm IN}$ and Z_X) and poloidal field null (B_r and B_z) variables are then determined by taking the pseudo-inverse of the plant matrix. The equilibrium controller design is implemented in feedback mode with respect to the shape variables, implying LEMUR drives the respective 'virtual circuits' with the estimation for the shape variables in real-time for feedback control during the scenario. Feedforward perturbations are applied by the PCS to drive B_r and B_z to zero at (0.7 m, −1.74 m), which in turn drives the corresponding 'virtual circuit' for controlling the poloidal magnetic field null.

Figures 8(*a*)–(*e*) show an example of the experimental application of the magnetic equilibrium controller for providing real-time feedback control of the plasma boundary ($R_{\rm OUT}$, $R_{\rm IN}$, Z_X) and feedforward control of the poloidal field components at (0.7 m, −1.74 m) for obtaining a 600 kA X-divertor plasma configuration, #48696. Note that this is the first time that a steady state X-divertor plasma configuration has been enabled on MAST-U. The activation time for LEMUR for estimating the boundary control variables starts at $T = 0.11$ s. The activation time interval for studying the dynamical response of the boundary control variables ($R_{\rm OUT}$, $R_{\rm IN}$ and Z_X) is shown in the green shaded regions in figures 8(*a*)–(*c*). They all illustrate a good tracking of the time varying pre-programmed reference for the boundary control variables upon activation of the feedback controller. Pre-programmed reference values of B_r and B_z perturbations are applied that comprises of a ramp target phase between $T = 0.3$ s and $T = 0.4$ s. Similar to the X-point target plasma case, the B_r and B_z perturbation values for the X-divertor configuration are obtained by evaluating the poloidal field components from the off-line EFITs at the desired secondary X-point from a previous discharge. The impact of the pre-programmed references on the evolution of the poloidal field components at (0.7 m, −1.74 m) is shown in figure 8(*d*). Note that the convergence to the performance in the discharge, #48696, was achieved at the expense of a sequence of tuning iterations over 3 plasma shots. The radial and vertical poloidal field components during the activation window of the feedforward controller approach values close to zero at $T = 0.4$ s

and result in a finite steady state offset. As already mentioned for X-point target case, the steady state performance can be improved by tuning the feedforward references over plasma discharges by accounting for model inaccuracies and disturbances. However, with the future availability of the real-time estimation of multiple X-point locations from LEMUR, the feedback control mode would provide solutions to these issues. Figure 8(*e*) shows the final steady state X-divertor configuration at $T = 0.5$ s. The off-line EFIT reconstruction at steady state estimates the secondary X-point position at (0.66 m, −1.71 m) in comparison to desired location of (0.7 m, −1.74 m).

5. Summary and conclusions

A new real-time magnetic equilibrium control design relying on the LEMUR algorithm has been developed particularly for advanced plasma configurations (double null conventional, Super-X, X-point target and X-divertors) and applied experimentally on MAST-U. The development of LEMUR and the associated magnetic equilibrium control design has not only improved the existing Super-X and Double null divertor plasma configurations by providing feedback and feedforward control of ($R_{\rm OUT}$, $R_{\rm IN}$, R_X, Z_X,$R_{\rm STK}$, $R_{\rm LEG}$ and $F_{\rm exp}$) but also enabled for the first time steady state divertor plasma configuration such as, X-point target and X-divertor plasmas. Comparisons are made of the equilibrium control parameters from LEMUR against off-line equilibrium reconstruction, based on the Grad–Shafranov solver and diagnostic measurements for MAST-U plasma configurations. Modelling, design and simulation of the axisymmetric magnetic equilibrium control scheme for plasma boundary and divertor leg for MAST-U, have been accomplished using the TokSys software suite. A non-linear free boundary plasma simulation (GSevolve) directly connected to the MAST-U PCS, has been used for the verification and identification of the control parameters. These capabilities also enable the TokSys software suite to perform off-line tests and assessments for studying the responses of the virtual circuits prior to the experimental implementation of the magnetic equilibrium controller. The MAST-U magnetic control approach described here results in good tracking, appropriate response times, and low steady state errors with respect to complex changes in the reference control variables during the experimental application, consistent with control performance requirement for advanced divertor plasma configurations. In particular for the Super-X divertor plasma configuration, the magnetic equilibrium controller shows good rejection performance with respect to pre-programmed disturbances and prevents contact of the separatrix with the divertor baffle during the controller activation period. With respect to the development of X-point target and X-divertor plasma configuration, the feedforward mode of the MAST-U magnetic controller was successful in generating and holding both the divertor configurations in steady state operation.

In the upcoming 2023–2024 MAST-U experimental campaign, demonstration of full feedback control is planned for all the advanced MAST-U divertor plasma configurations. As a step towards this development, LEMUR algorithm upgrades are planned to enable real-time estimation of the poloidal flux expansion at the divertor target and multiple X-point positions in the divertor chamber, along with plasma parameters including plasma inductance, l_i and plasma poloidal beta, β_p. The successful feedforward control demonstration in the current 2022–2023 MAST-U experimental campaign for various parameters that were not currently computed in real-time by LEMUR lays a strong foundation for feedback control tests with real-time availability of magnetic control variables in the future campaigns. The MAST-U magnetic controller is also planned to be extended to other advanced plasma configurations, such as, negative triangularity divertors and snowflake divertors [39]. During the current shutdown period, the control development for these plasma configurations will rely on SIL simulations, making use of the GA-TokSys simserver platform. The MAST-U magnetic equilibrium controller design with the integrated control approach discussed in the paper will provide high confidence control verification prior to operational use and is expected to increase the probability of success within limited experimental operation time for new advanced plasma configurations and scenarios in the upcoming 2023–2024 MAST-U experimental campaign. The successful application of the GA-TokSys integrated control approach and experimental validation on MAST-U also provides high confidence in the value of this approach to other devices anticipated to begin operation in the near- and medium-term (e.g. NSTX-U, STEP).

Acknowledgments

This material is based upon work supported by the U.S. Department of Energy, Office of Science, Office of Fusion Energy Sciences, using the MAST-U Fusion Facility, under Awards DE-SC0018991, DE-AC05-00OR22725 and DE-AC52-07NA27344.

This work has been (part-) funded by the EPSRC Energy Programme [Grant Number EP/W006839/1].

Disclaimer

ORCID iDs

H. Anand https://orcid.org/0000-0002-9632-5680
D. Eldon https://orcid.org/0000-0003-1895-0648
A. Lvovskiy https://orcid.org/0000-0002-3649-1169
J. Barr https://orcid.org/0000-0001-7768-5931
N. Eidietis https://orcid.org/0000-0003-0167-5053
A. Leonard https://orcid.org/0000-0001-9356-1074
G. McArdle https://orcid.org/0000-0003-0888-0105
J. Harrison https://orcid.org/0000-0003-2906-5097
V. Soukhanovskii https://orcid.org/0000-0001-5519-0145
J. Lovell https://orcid.org/0000-0001-9565-3466

References

[1] Fishpool G., Canik J., Cunningham G., Harrison J., Katramados I., Kirk A., Kovari M., Meyer H. and Scannell R. 2013 MAST-upgrade divertor facility and assessing performance of long-legged divertors *J. Nucl. Mater.* **438** S356
[2] Valanju P.M., Kotschenreuther M., Mahajan S.M. and Canik J. 2009 Super-X divertors and high power density fusion devices *Phys. Plasma* **16** 056110
[3] Umansky M.V., Rensink M.E., Rognlien T.D., LaBombard B., Brunner D., Terry J.L. and Whyte D.G. 2017 Assessment of X-point target divertor configuration for power handling and detachment front control *Nucl. Mater. Energy* **12** 918
[4] Reimerdes H. *et al* 2017 TCV divertor upgrade for alternative magnetic configurations *Nucl. Mater. Energy* **12** 1106
[5] Reimerdes H. *et al* 2020 Assessment of alternative divertor configurations as an exhaust solution for DEMO *Nucl. Fusion* **60** 066030
[6] Walker M.L. and Humphreys D.A. 2006 Valid coordinate systems for linearized plasma shape response models in tokamaks *Fusion Sci. Technol.* **50** 473
[7] Ferron J.R., Walker M.L., Lao L.L., John H.E.S., Humphreys D.A. and Leuer J.A. 1998 Real time equilibrium reconstruction for tokamak discharge control *Nucl. Fusion* **38** 1055
[8] Moret J.-M., Duval B.P., Le H.B., Coda S., Felici F. and Reimerdes H. 2015 Tokamak equilibrium reconstruction code LIUQE and its real time implementation *Fusion Eng. Des.* **91** 1
[9] Barana O., Joffrin E., Murari A. and Sartori F. 2003 Real-time determination of confinement parameters in JET *Fusion Eng. Des.* **66–68** 697
[10] Albanese R. *et al* 2016 A MIMO architecture for integrated control of plasma shape and flux expansion for the EAST tokamak *2016 IEEE Conf. Control Appl. CCA* (*September 2016*) p 611
[11] Anand H., Coda S., Felici F., Galperti C. and Moret J.-M. 2017 A novel plasma position and shape controller for advanced configuration development on the TCV tokamak *Nucl. Fusion* **57** 126026
[12] Boyer M.D. *et al* 2018 Plasma boundary shape control and real-time equilibrium reconstruction on NSTX-U *Nucl. Fusion* **58** 36016
[13] Allegra C.J. *et al* 2009 Design of plasma shape control system for KSTAR tokamak *2009 23rd IEEE/NPSS Symp. on Fusion Engineering* pp 1–4
[14] Yuan Q.P. *et al* 2013 Plasma current, position and shape feedback control on EAST *Nucl. Fusion* **53** 43009
[15] Treutterer W. *et al* 1997 Plasma shape control design in ASDEX upgrade *Fusion Technology 1996* ed C. Varandas and F. Serra (Elsevier) pp 933–6
[16] Tommasi G., Albanese R., Ambrosino G. and Ariola M. 2007 XSC tools: a software suite for tokamak plasma shape control design and validation *IEEE Trans. Plasma Sci.* **35** 709
[17] Ambrosino G., Ariola M., De Tommasi G., Pironti A. and Portone A. 2009 Design of the plasma position and shape control in the ITER tokamak using in-vessel coils *IEEE Trans. Plasma Sci.* **37** 1324
[18] Humphreys D.A. and Hutchinson I.H. 1993 Axisymmetric magnetic control design in tokamaks using perturbed equilibrium plasma response modeling *Fusion Technol.* **23** 167
[19] Pangione L., Mcardle G. and Storrs J. 2013 New magnetic real time shape control for MAST *Fusion Eng. Des.* **88** 1087
[20] Anand H., Eldon D., Kochan M., McArdle G., Pangione L. and Wang H.Q. 2022 Validation of the strike point position estimation with the local expansion method for MAST upgrade on the DIII-D tokamak *Fusion Eng. Des.* **177** 113086
[21] Kochan M. *et al* 2023 Real-time plasma shape reconstruction on MAST upgrade based on local expansion *30th IEEE Symosium on Fusion Engineering* (https://doi.org/10.1542/neo.24-11-e748)
[22] Guo Y., Xiao B. and Luo Z. 2011 A local expansion method applied to fast plasma boundary reconstruction for EAST *Plasma Phys. Control. Fusion* **53** 105015
[23] Humphreys D.A., Ferron J.R., Hyatt A.W., La Haye R.J., Leuer J.A., Penaflor B.G., Walker M.L., Welander A.S. and In Y. 2008 DIII-D integrated plasma control solutions for ITER and next-generation tokamaks *Fusion Eng. Des.* **83** 193
[24] Luxon J.L. 2002 A design retrospective of the DIII-D tokamak *Nucl. Fusion* **42** 614
[25] Lee G.S. *et al* (KSTAR Team) 2001 Design and construction of the KSTAR tokamak *Nucl. Fusion* **41** 1515
[26] Li J. *et al* 2013 A long-pulse high-confinement plasma regime in the experimental advanced superconducting tokamak *Nat. Phys.* **9** 817
[27] Walker M.L. *et al* 2015 The ITER plasma control system simulation platform *Fusion Eng. Des.* **96–97** 716–9
[28] Anand H., Bardsley O., Humphreys D., Lennholm M., Welander A., Xing Z., Barr J., Walker M., Mitchell J. and Meyer H. 2023 Modelling, design and simulation of plasma magnetic control for the Spherical Tokamak for Energy Production (STEP) *Fusion Eng. Des.* **194** 113724
[29] Mcardle G., Pangione L. and Kochan M. 2020 The MAST Upgrade plasma control system *Fusion Eng. Des.* **159** 111764
[30] Lao L.L., John H.E.S., Peng Q., Ferron J.R., Strait E.J., Taylor T.S., Meyer W.H., Zhang C. and You K.I. 2005 MHD equilibrium reconstruction in the DIII-D tokamak *Fusion Sci. Technol.* **48** 968
[31] Kogan L. *et al* 2022 First MAST-U equilibrium reconstructions using the EFIT++ code *48th EPS Conf. Plasma Physics, EPS 2022* p 2
[32] Knolker M., Osborne T., Belli E., Henderson S., Kirk A., Kogan L., Saarelma S. and Snyder P.B. 2021 Pedestal stability analysis on MAST in preparation for MAST-U *Nucl. Fusion* **61** 046041
[33] Ryan P.J., Elmore S.D., Harrison J.R., Lovell J. and Stephen R. 2023 Overview of the langmuir probe system on the mega ampere spherical tokamak (MAST) upgrade *Rev. Sci. Instrum.* **94** 103501

[34] Wijkamp T. *et al* (the MAST Upgrade team) 2023 Characterisation of detachment in the MAST-U Super-X divertor using multi-wavelength imaging of 2D atomic and molecular emission processes *Nucl. Fusion* **63** 056003
[35] Anand H., Humphreys D., Eldon D., Leonard A., Hyatt A., Sammuli B. and Welander A. 2021 Plasma flux expansion control on the DIII-D tokamak *Plasma Phys. Control. Fusion* **63** 015006
[36] Welander A., Olofsson E., Sammuli B., Walker M.L. and Xiao B. 2019 Closed-loop simulation with Grad-Shafranov equilibrium evolution for plasma control system development *Fusion Eng. Des.* **146** 2361
[37] Welander A.S., Deranian R.D., Humphreys D.A., Leuer J.A. and Walker M.L. 2005 Nonrigid, linear plasma response model based on perturbed equilibria for axisymmetric tokamak control design *Fusion Sci. Technol.* **47** 763
[38] Sykes A *et al* 1993 Tight aspect ratio tokamaks—Theory and experiment *Plasma Phys. Control. Fusion* (https://doi.org/10.1088/0741-3335/35/8/011)
[39] Soukhanovskii V.A., Cunningham G., harrison J.R., Federici F. and Ryan P. 2022 First snowflake divertor experiments in MAST-U tokamak *Nucl. Mater. Energy* **33** 101278